UNIVERSITY *of* York

This is a repository copy of *Nonperturbative approach to interfacial spin-orbit torques induced by the Rashba effect*.

Nonperturbative approach to interfacial spin-orbit torques induced by the Rashba effect

Alessandro Veneri ⬤, David T. S. Perkins ⬤, and Aires Ferreira ⬤*

School of Physics, Engineering and Technology and York Centre for Quantum Technologies,
University of York, YO10 5DD, York, United Kingdom

Current-induced spin-orbit torque (SOT) in normal metal/ferromagnet (NM/FM) bilayers bears great promise for the development of low-power spin-based devices, but the microscopic origin of purely interfacial SOTs in ultrathin systems is not yet fully understood. Here, we show that a linear response theory with a nonperturbative treatment of spin-dependent interactions and impurity scattering potential predicts dampinglike (DL) SOTs that are strictly absent in perturbative approaches. The technique is applied to a two-dimensional Rashba-coupled FM (the paradigmatic model of a NM/FM interface), where higher-order scattering processes encoding skew scattering from nonmagnetic impurities allow for current-induced spin polarization with nonzero components along all spatial directions. This is in stark contrast to previous results of perturbative methods (neglecting skew scattering), which predict a coplanar spin-polarization locked perpendicular to the charge current as a result of the conventional Rashba-Edelstein effect. Furthermore, the angular dependence of ensuing SOTs and their dependence upon the scattering potential strength is analyzed numerically. Simple analytic expressions for the spin-density–charge-current response function and related SOT efficiencies are obtained in the weak scattering limit. We find that the extrinsic DL torques driven by impurity scattering reaches efficiencies of up to 7% of the fieldlike (Rashba-Edelstein) torque. Our microscopic theory shows that bulk phenomena, such as the spin Hall effect, are not a necessity in the generation of the DL SOTs of the type observed in experiments on ultrathin systems.

I. INTRODUCTION

Spin-orbit torque (SOT) [1] is a phenomenon in which an unpolarized charge current injected into a normal metal/ferromagnetic metal (NM/FM) bilayer with inversion symmetry-breaking spin-orbit coupling (SOC) induces a nonequilibrium spin density $\mathbf{S}$ in the NM and hence a torque $\mathbf{T} \propto \mathbf{S} \times \mathbf{M}$. This torque then drives the dynamics of the magnetization of the FM layer $\mathbf{M}$, which can be switched by an electric current from one static configuration to another or enter into steady-state precession [2]. Such spin-torque-driven magnetization dynamics offers up a plethora of spintronic applications [3–6]. In comparison with spin-transfer torque devices [2], SOT allows for faster and more energy-efficient devices [4,7–9].

Interfacial SOTs (i.e., those associated with purely interfacial effects) can arise from the lack of inversion symmetry in the stacking direction of NM/FM bilayers [1], which yields charge-to-spin conversion (CSC) processes, resulting in the appearance of a spin accumulation in the NM at the interface—a transport phenomenon commonly referred to as the Rashba-Edelstein effect (REE) [10–12]. In this scenario, a charge current passing through the NM layer generates a spin accumulation $\mathbf{S}$ at the surface of the material at the interface of the bilayer [13], which then exerts a torque on the magnetization of the FM partner due to the proximity coupling between itinerant electron spins and localized spins. Broadly speaking, two types of SOT can be generated: the first is

called *dampinglike* (DL) SOT, which tends to align $\mathbf{M}$ with the effective magnetic field $\mathbf{H}_{\mathrm{eff}}$, acting upon the local magnetic moments of the FM (this comprises the demagnetization field, anisotropy field, and any applied external magnetic fields [1]). The second type of torque is called *fieldlike* (FL) SOT, which causes $\mathbf{M}$ to precess about $\mathbf{H}_{\mathrm{eff}}$. It is common practice in the literature to identify these torques by their odd/even nature in the magnetization, that is, $\mathbf{T}_{\mathrm{DL}} \equiv \mathbf{T}_{\mathrm{e}}$ and $\mathbf{T}_{\mathrm{FL}} \equiv \mathbf{T}_{\mathrm{o}}$ with $\mathbf{T}_{\mathrm{e}}(\mathbf{M}) = \mathbf{T}_{\mathrm{e}}(-\mathbf{M})$ and $\mathbf{T}_{\mathrm{o}}(\mathbf{M}) = -\mathbf{T}_{\mathrm{o}}(-\mathbf{M})$. While we have introduced this convention here, we would like to note that this is only strictly true for specific torque terms that appear to leading order in the magnetization, namely, the conventional FL SOT ($\mathbf{T}_{\mathrm{FL}} \propto \mathbf{M} \times \hat{y}$) and DL SOT ($\mathbf{T}_{\mathrm{DL}} \propto \mathbf{M} \times \mathbf{M} \times \hat{y}$, for a charge current applied along $\hat{x}$). However, a rigorous determination of the DL and FL torques can be achieved via a vector spherical harmonics expansion [14]. For simplicity though, we shall use the common naming convention of the SOT types.

In practice, there are two main mechanisms driving SOTs at NM/FM bilayers: the spin Hall effect (SHE) appearing in the bulk of the NM and the REE appearing at the interface. A phenomenological study, along with a perturbative semiclassical Boltzmann analysis, of the SOTs generated by the SHE and REE was presented in Ref. [15]. In that work, they observed that both the DL and FL torques stemming from the SHE became vanishingly small as the system thickness was decreased (the SHE is effectively suppressed when the spin diffusion length exceeds the NM thickness [16,17]). In contrast, only the DL torque of the interfacial REE became negligible in the ultrathin limit, while the FL torque of the REE remained approximately constant. However, several

235419-1

experiments on thin bilayers have observed torques that cannot be captured purely by the SHE, thus indicating the presence of significant interfacial DL torques [18,19]. In fact, authors of a study of an ultrathin metallic bilayer (with a thickness <1 nm), where SHE contributions are vanishingly small, still observed nonnegligible DL torques responsible for the magnetic switching of the FM, whose origin must be the interface [19]. Meanwhile, microscopic theories of interfacial SOTs have been put forward [20–23], though they have still failed to capture DL torques large enough to explain experimental observation in ultrathin NM/FM bilayers [19] as well as the anisotropy of the DL torque [18]. Although these microscopic models handled the important role played by disorder in the NM, they did so within the Gaussian (white-noise) approximation where the scattering potential is treated perturbatively, while also treating the magnetic exchange interaction between conduction electrons and the FM localized spins in a similar manner. The key finding of these early studies is the *complete absence of DL torques* in the two-dimensional Rashba-coupled FM model, once vertex corrections due to impurity scattering are accounted for in a consistent way [21].

The use of perturbative methods has been questioned in a recent study [24], where strong impurity scattering and the rich evolution of equilibrium spin textures with the Fermi level were seen to play a crucial role in the buildup of nonequilibrium spin polarization and associated SOTs in van der Waals heterostructures. Motivated by these developments, in this paper, we shed light on the microscopic origin of interfacial SOTs in diffusive metallic bilayers and demonstrate that *DL torques with nontrivial angular dependence* can be generated purely at the interface due to the interplay of Rashba SOC, the magnetic proximity effect, and impurity scattering. To this end, we formulate a linear response theory that is nonperturbative in both the impurity scattering strength and spin interactions (magnetic exchange and Rashba SOC) to calculate the current-induced spin polarization in the NM, **S**. We achieve this by modeling the NM as a two-dimensional electron gas (2DEG) and employ a generalized self-consistent diagrammatic technique that handles disorder at the complete T-matrix level [25–29] to calculate the spin-density–charge-current response functions, while allowing for the magnetization of the FM to lie at an arbitrary angle. The anisotropic spin texture of the Fermi rings of the 2DEG can be seen to enrich the possible current-induced spin polarizations (with hitherto unseen nonzero components along all principal axes emerging as a result of skew scattering of conduction electrons), and hence, we predict alternative types of interfacial SOT with extrinsic origin. We present analytical results in the weak scattering limit (WSL; incorporating skew scattering) and use a numerical procedure to extract the full angular dependence of the SOTs.

The remainder of this paper is structured as follows: In Sec. II, we formally introduce current-induced SOTs exerted by the NM and the Hamiltonian for disordered 2DEGs with symmetry-breaking SOC. We then present a self-consistent diagrammatic theory to evaluate the disorder-averaged linear response by making use of the T-matrix approach. Afterwards, in Sec. III, we provide an intuitive semiclassical picture for the SOT in NM/FM bilayers before then applying the diagrammatic method to 2DEGs in the weak scattering limit.

Additionally, we provide a numerical study of the SOT in the strong scattering limit as well as the dependence of the SOT coefficients upon the orientation of the magnetization. In Sec. IV, we present our conclusions. Technical details of the calculations are relegated to the Appendix.

II. MODELS AND METHODS

A. SOT components and notation

The dynamical effects of SOT can be modeled by including the additive term [1]:

$$\mathbf{T} = \frac{\gamma}{d\,M_s}\mathbf{H}_{\text{SOT}} \times \mathbf{m},\tag{1}$$

into the Landau-Lifshitz-Gilbert equation [5], where d is thickness of the FM, $\mathbf{m} = \frac{\mathbf{M}}{M_s}$ is the unit magnetization vector (with $M_s = |M|$ the saturation magnetization of the FM layer), γ is the gyromagnetic ratio, and $\mathbf{H}_{\text{SOT}}$ is the effective magnetic field [Eq. (2)] generated by the nonequilibrium spin polarization of conduction electrons. Within the theory of linear response, we may write the effective field as

$$\mathbf{H}_{\text{SOT}} = \Delta_{\text{xc}}\hat{K}\,\mathbf{E},\tag{2}$$

where Δ_{xc} is the interfacial exchange coupling, and $\hat{K}$ is the spin susceptibility tensor, and $\mathbf{E}$ is the external electric field.

To separate the torque term in Eq. (1) into DL (even in **m**) and FL (odd in **m**) parts $\mathbf{T}^{\text{e}}$ and $\mathbf{T}^{\text{o}}$, respectively, we perform a symmetry analysis based on the following decomposition for a magnetization taken to be in the xz-plane

$$\mathbf{T}^{\text{e}} = \frac{\Delta_{\text{xc}}\gamma}{d\,M_s}\{t_1^{\text{e}}\mathbf{m} \times [\mathbf{m} \times (\mathbf{e}_z \times \mathbf{E})] + t_2^{\text{e}}\mathbf{m} \times \mathbf{e}_z(\mathbf{m} \cdot \mathbf{E})\},\tag{3a}$$

$$\mathbf{T}^{\text{o}} = \frac{\Delta_{\text{xc}}\gamma}{d\,M_s}[t_1^{\text{o}}\mathbf{m} \times (\mathbf{e}_z \times \mathbf{E}) + t_2^{\text{o}}\mathbf{m} \times (\mathbf{m} \times \mathbf{e}_z)(\mathbf{m} \cdot \mathbf{E})],\tag{3b}$$

which assumes the low-energy (long-wavelength) Hamiltonian of the NM system to possess continuous rotational symmetry about the z axis in the absence of magnetic exchange proximity effects. This is a valid assumption in devices fabricated from polycrystalline and disordered samples [18,30–33] but is also expected to hold certainly in atomically sharp interfaces with high symmetry (e.g., as realized in van der Waals heterostructures [24]). The torque coefficients $t_i^j \equiv t_i^j(\mathbf{m})$ are the controlling parameters of SOT and hence are the primary focus of this paper. The torque efficiencies may be written in terms of the magnetization and spin susceptibility tensor components as

$$t_1^{\text{e}} = \frac{K_{yy}}{m_z},\tag{4a}$$

$$t_2^{\text{e}} = \frac{K_{xx} - K_{yy}}{m_x^2 m_z} - \frac{K_{xx}}{m_z} - \frac{K_{zx}}{m_x},\tag{4b}$$

$$t_1^{\text{o}} = K_{xy} - \frac{m_x}{m_z}K_{zy},\tag{4c}$$

$$t_2^{\text{o}} = \frac{1}{m_x}\left(\frac{K_{xy} + K_{yx}}{m_x} - \frac{K_{zy}}{m_z}\right).\tag{4d}$$

From these expressions, we clearly see that K_{xx}, K_{yy}, and K_{zx} contribute solely to the DL torque, while K_{xy}, K_{yx}, and K_{zy} generate the FL torque.

B. The Hamiltonian

The general Hamiltonian for the FM partner material may be written as

$$\mathcal{H} = \mathcal{H}_0 + \mathcal{H}_{\text{PE}} + \mathcal{H}_{\text{dis}}, \tag{5}$$

where $\mathcal{H}_0$ is the Hamiltonian for the clean isolated NM, $\mathcal{H}_{\text{PE}}$ accounts for proximity effects, and $\mathcal{H}_{\text{dis}}$ describes the impurity landscape. In this paper, we model the NM as a 2DEG, while focusing on the effects of Rashba SOC and the exchange interaction between classical magnetic moments in the FM and the spin of conduction electrons in the NM. We may therefore write $\mathcal{H}_{\text{PE}} = \mathcal{H}_{\text{BR}} + \mathcal{H}_{\text{xc}}$, where the first and second terms correspond to Rashba SOC and the exchange interaction, respectively. To describe the spin-dependent interactions in a compact form, we introduce the non-Abelian SU(2) gauge field [34]:

$$\mathcal{A}^{\mu} = \mathcal{A}_i^{\mu} s_i \quad (i = 0, x, y, z), \tag{6}$$

where s_i $(i = x, y, z)$ are Pauli matrices acting in spin space, and s_0 is the identity matrix. This field is then inserted into $\mathcal{H}_0$ as a generalized vector potential in an analogy to minimal coupling. For a standard Rashba-coupled FM, we have only the nonzero components being

$$\mathcal{A}_x^y = -\mathcal{A}_y^x = \alpha m^*, \quad \mathcal{A}^0 = -\Delta_{\text{xc}} \mathbf{m} \cdot \mathbf{s} \equiv -\boldsymbol{\Delta} \cdot \mathbf{s}, \tag{7}$$

where m^* is the effective electron mass, α is the SOC strength, and Δ_{xc} is the exchange coupling (here, we assumed a conventional isotropic Zeeman interaction [35]).

In the absence of disorder, the NM Hamiltonian takes the second-quantized form:

$$\mathcal{H}_0 + \mathcal{H}_{\text{PE}} = \int d\mathbf{x}\, \psi^{\dagger}(\mathbf{x}) \left[\frac{(\mathbf{p} + \boldsymbol{\mathcal{A}})^2 - \boldsymbol{\mathcal{A}}^2}{2m^*} - \varepsilon - \mathcal{A}^0 \right] \psi(\mathbf{x}). \tag{8}$$

Here, ε is the Fermi energy, and $\mathbf{p}$ is the 2D momentum operator. The disorder term in the Hamiltonian $\mathcal{H}_{\text{dis}}$ reads as

$$\mathcal{H}_{\text{dis}} = \int d\mathbf{x}\, \psi^{\dagger}(\mathbf{x}) V(\mathbf{x}) \psi(\mathbf{x}), \tag{9a}$$

$$V(\mathbf{x}) = \sum_i W(\mathbf{x} - \mathbf{x}_i), \tag{9b}$$

where $V(\mathbf{x})$ is the total impurity potential, and $W(\mathbf{x} - \mathbf{x}_i)$ is the potential of a single impurity located at position $\mathbf{x}_i$ within the NM/FM interface (the areal density of impurities is denoted as n). We note that, in general, $V(\mathbf{x})$ has a matrix structure and can include effects such as local SOC and magnetic impurities [36], but these are not a necessity in the generation of FL and DL SOTs, as we shall show below. To recover macroscopic results, we average over all possible impurity configurations within the T-matrix formalism [25], which accounts for all possible scattering scenarios involving a single impurity. In this paper, we work in the dilute limit ($n \ll 1$) with a focus on short-range scalar impurities: $W(\mathbf{r}) = uR^2 \delta(\mathbf{r})$, where u is the scattering potential, R is

the characteristic length scale of the range of the impurity potential, and $\delta(\mathbf{r})$ is the delta (Dirac) function.

Having set up the Hamiltonian describing the NM, our focus now turns to calculating the generalized spin-density–charge-current response tensor. The next section details our theory for obtaining response functions without the need for a perturbative treatment of the exchange coupling, Rashba SOC, or impurity scattering potential. The only perturbative parameter governing the validity of our diagrammatic theory is $(\varepsilon\tau)^{-1} \ll 1$, where τ is the momentum relaxation time.

C. Diagrammatic theory and the *T*-matrix

To understand the response of a system to spin-charge conversion away from equilibrium, we employ the theory of linear response. We assume that $\mathbf{M}$ and $\mathbf{E}$ vary slowly in both position and time (i.e., on scales larger than the mean free path and τ) and hence neglect their spatial and temporal dependence. The response of the spin density to the electric field is then simply (assuming Einstein summation)

$$S_{\alpha} = K_{\alpha\beta} E_{\beta}, \tag{10}$$

where $K_{\alpha\beta}$ ($\alpha = x, y, z$ and $\beta = x, y$) is the spin-susceptibility response tensor with a 3×2 matrix structure in our case [c.f. Eq. (2)]. Therefore, the effect of SOT upon the FM is contained entirely within the object $K_{\alpha\beta}$, which we shall treat using the Kubo-Streda formula [37]. This spin-current response function can be separated into two contributions:

$$K_{\alpha\beta} = R_{\alpha\beta}^0 + R_{\alpha\beta}^{\varepsilon}, \tag{11}$$

where $R_{\alpha\beta}^0$ is the Fermi sea (type II) response of the system, and $R_{\alpha\beta}^{\varepsilon}$ is the Fermi surface (type I) contribution to the total response. Written explicitly, the Fermi surface response takes the form:

$$R_{\alpha\beta}^{\epsilon} = -\frac{1}{4\pi} \langle \text{Tr}[(s_{\alpha} G^+ j_{\beta} - j_{\beta} G^- s_{\alpha})(G^+ - G^-)] \rangle_{\text{dis}}, \tag{12}$$

where $j_{\beta} = e\, \partial\mathcal{H}/\partial p_{\beta}$ is the electric current operator [38] ($e < 0$), $\langle...\rangle_{\text{dis}}$ denotes disorder averaging, $G^{\pm} = (\epsilon - \mathcal{H} \pm i\delta)^{-1}$ is the clean retarded ($+$)/advanced ($-$) Green's function at the Fermi surface, and δ is a positive infinitesimal. By working in the dilute limit (i.e., low impurity concentration), we may neglect the Fermi sea contribution and ignore terms containing products of the same Green's function in Eq. (12) [25]:

$$K_{\alpha\beta} \simeq \frac{1}{2\pi} \text{Tr}[\langle s_{\alpha} G^+ j_{\beta} G^- \rangle_{\text{dis}}]. \tag{13}$$

Applying the disorder average yields

$$K_{\alpha\beta} = \frac{1}{2\pi} \sum_{\mathbf{p}} \text{tr}[\tilde{s}_{\alpha} \mathcal{G}_{\mathbf{p}}^+ j_{\beta} \mathcal{G}_{\mathbf{p}}^-], \tag{14}$$

where we have written the response function in momentum space explicitly, and the trace is now over the internal matrix indices. We perform our calculations using the standard rules of diagrammatics and assume the noncrossing approximation [39]. The retarded and advanced disorder-averaged
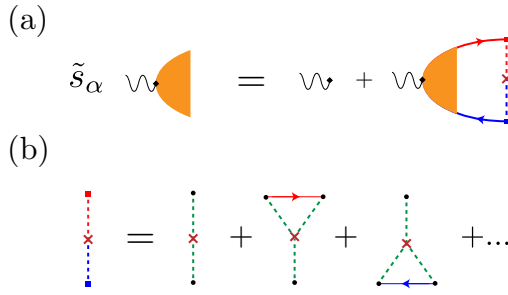
FIG. 1. Diagrammatic expansion of the zero-temperature spin-density–charge-current response function: (a) the disorder-renormalized spin density vertex function and (b) the T-matrix skeleton expansion. Solid lines with arrows denote disorder averaged Green's functions, while green dashed lines represent single impurity potential insertions. Red/blue indicates advanced/retarded sectors.

Green's functions appearing in Eq. (14) are given by

$$\mathcal{G}_\mathbf{p}^\pm = \frac{1}{(G_{0,\mathbf{p}}^\pm)^{-1} - \Sigma^\pm}, \tag{15}$$

where $G_{0,\mathbf{p}}^\pm$ is the clean Green's function, and $\Sigma^\pm$ is the retarded/advanced disorder self-energy. To leading order in the impurity density n, we may relate $\Sigma^\pm$ to the T-matrix via $\Sigma^\pm = nT^\pm$. The advanced/retarded T-matrix is represented diagrammatically in Fig. 1, which can be shown to yield

$$T^\pm = \widetilde{W} \frac{1}{1 - \widetilde{W} g_0^\pm}, \tag{16a}$$

$$g_0^\pm = \int \frac{d^2p}{(2\pi)^2} G_{0,\mathbf{p}}^\pm, \tag{16b}$$

where $g_0^\pm$ is the momentum-integrated clean Green's function, and $\widetilde{W}$ is the Fourier transform of $W(\mathbf{r})$. Finally, the renormalized vertex $\tilde{s}_\alpha$ (Fig. 1) is given by the Bethe-Salpeter equation [40]:

$$\tilde{s}_\alpha = s_\alpha + n \sum_\mathbf{p} T^- \mathcal{G}_\mathbf{p}^- \tilde{s}_\alpha \mathcal{G}_\mathbf{p}^+ T^+. \tag{17}$$

Within the first Born approximation (FBA), Eq. (16a) is expanded to second order in W. This leads to the renormalized vertex being given by a simple ladder series of impurity scatterings and hence fails to capture the physics of skew scattering. This is represented by the first term in Fig. 1(b). We must therefore perform a T-matrix expansion that is nonperturbative in the scattering potential [41,42].

A common approximation accompanying the FBA is the Gaussian approximation, in which off-diagonal elements in the FBA (recall we are working with 2×2 spin matrices) are also neglected. However, we note that, even with scalar impurities, Eq. (16a) allows for the T-matrix to possess nonzero off-diagonal elements. Therefore, to create a fully self-consistent theory, we must include these elements, and so the Gaussian approximation is not appropriate for understanding the nonequilibrium spin density induced in the NM.

To account for all terms and the matrix structure of $T^\pm$, we employ a method like that of Refs. [28,43] to simplify

the renormalized vertex by projecting Eq. (17) onto the Pauli algebra (here, $\alpha, \beta, \nu \in \{0, x, y, z\}$):

$$\tilde{s}_\alpha = \mathcal{D}_{\alpha\beta} s_\beta, \quad \mathcal{D}_{\alpha\beta} = \tfrac{1}{2}\text{tr}[\tilde{s}_\alpha s_\beta]. \tag{18}$$

The coefficients are then given by

$$\mathcal{D}_{\alpha\beta} = \delta_{\alpha\beta} + \mathcal{D}_{\alpha\nu}\mathcal{M}_{\nu\beta},$$
$$\mathcal{M}_{\nu\beta} = \frac{n}{2} \sum_\mathbf{p} \text{tr}[T^- \mathcal{G}_\mathbf{p}^- s_\nu \mathcal{G}_\mathbf{p}^+ T^+ s_\beta]. \tag{19}$$

To evaluate the $\mathcal{M}$-matrix, we decompose it into two separate matrices:

$$\Upsilon_{\alpha\beta} = \frac{1}{2}\text{tr}[s_\alpha T^+ s_\beta T^-], \quad \mathcal{N}_{\alpha\beta} = \frac{n}{2} \sum_\mathbf{p} \text{tr}[s_\alpha \mathcal{G}_\mathbf{p}^+ s_\beta \mathcal{G}_\mathbf{p}^-], \tag{20}$$

such that $\mathcal{M} = \mathcal{N}\Upsilon$. The Υ-matrix describes the insertion of impurities connecting the two sides of the response bubble, while the $\mathcal{N}$-matrix encodes information about the disorder-averaged Green's functions forming a response bubble in the absence of interference.

The projection coefficients are in fact the elements of the generalized Diffuson operator:

$$\mathcal{D} = (1 - \mathcal{M})^{-1}. \tag{21}$$

Consequently, Eq. (14) becomes

$$K_{\alpha\beta} = \frac{1}{2\pi} \sum_\mathbf{p} \text{tr}[\mathcal{D}_{\alpha\nu} s_\nu \mathcal{G}_\mathbf{p}^+ j_\beta \mathcal{G}_\mathbf{p}^-]. \tag{22}$$

Under the Gaussian approximation, Υ becomes the sum over all forms of scalar disorder, reducing the generalized Diffuson to the standard form in the literature [44].

Finally, to find $\hat{K}_J$, we need to perform an analogous treatment of the current-current response function to obtain the charge conductivity tensor. In this case, the response function is given by Eq. (13) with $s_\alpha \to j_\alpha$. Upon disorder averaging, we now choose to renormalize the j_β vertex to yield

$$\sigma_{\alpha\beta} = \frac{1}{2\pi} \sum_\mathbf{p} \text{tr}[j_\alpha \mathcal{G}_\mathbf{p}^+ \tilde{j}_\beta \mathcal{G}_\mathbf{p}^-]. \tag{23}$$

The renormalized current vertex is found by letting $\tilde{j}_\beta = j_\beta + \delta j_\beta$ and then solving a Bethe-Salpeter equation for the corrections to the bare current vertex:

$$\delta j_\beta = \delta \bar{j}_\beta + n \sum_\mathbf{p} T^- \mathcal{G}_\mathbf{p}^- \delta j_\beta \mathcal{G}_\mathbf{p}^+ T^+, \tag{24a}$$

$$\delta \bar{j}_\beta = n \sum_\mathbf{p} T^- \mathcal{G}_\mathbf{p}^- j_\beta \mathcal{G}_\mathbf{p}^+ T^+. \tag{24b}$$

Since we are working with the current vertex explicitly, we use the projection:

$$\delta j_\beta = \widetilde{\mathcal{D}}_{\beta\nu} \delta \bar{j}_\nu, \quad \widetilde{\mathcal{D}}_{\beta\nu} = \tfrac{1}{2}\text{tr}[\delta j_\beta \delta \bar{j}_\nu], \tag{25}$$

and find an operator analogous to the Diffuson,

$$\widetilde{D} = (1 - \mathcal{N}^\text{T}\Upsilon^\text{T})^{-1}. \tag{26}$$

The electrical conductivity tensor is thus given by

$$\sigma_{\alpha\beta} = \frac{1}{2\pi} \sum_{\mathbf{p}} \text{tr}[j_\alpha \mathcal{G}_{\mathbf{p}}^+ (j_\nu + \widetilde{\mathcal{D}}_{\beta\nu} \delta \bar{j}_\nu) \mathcal{G}_{\mathbf{p}}^-]. \quad (27)$$

Given the expressions for the spin susceptibility and electrical conductivity in Eqs. (22) and (27), respectively, we may compute the spin-density response to the application of a charge current and hence calculate the effective magnetic field induced by the nonequilibrium spin density. This therefore provides us with a framework to determine the explicit form of the SOT [Eq. (2)] driving the magnetization dynamics of the FM. The efficiency of this charge-to-spin conversion (CSC) process can be defined as $\theta_{\alpha\beta} = -2ev K_{\alpha\beta}/\sigma_{xx}$, where v is the Fermi velocity and σ_{xx} is the longitudinal DC conductivity [45].

III. RESULTS AND DISCUSSION

Starting from the disorder-free electron picture of a 2DEG, Rashba SOC causes spin splitting of the parabolic dispersion into two bands with the spin of the electrons being locked in-plane and perpendicular to their momentum. The spins of the upper and lower bands (ν is the band index) wind in a clockwise and anticlockwise manner, respectively, around their corresponding Fermi rings. Next, the out-of-plane exchange interaction due to m_z opens a gap between the two bands and leads to an out-of-plane tilting in the spin texture of each band: the upper band spins rotate toward $m_z \mathbf{e}_z$, and the lower band spins rotate toward $-m_z \mathbf{e}_z$. Finally, the in-plane magnetization deforms the shape of the bands, while also shifting them in opposite directions along the axis perpendicular to the in-plane component. This generates a highly anisotropic dispersion relation, see Fig. 2, and so requires expansion in m_x and m_y to allow for analytic evaluation. For ease of analysis, as stated in Sec. II A, we work in a reference frame such that $m_y = 0$

$$\mathbf{m} = \sin\theta \, \mathbf{e}_x + \cos\theta \, \mathbf{e}_z. \quad (28)$$

Applying an electric field $\mathbf{E}$ to this system shifts the Fermi rings in the direction of $-\mathbf{E}$, leading to a nonzero center-of-mass momentum and hence an electrical current. This shifting of the Fermi rings leads to an out-of-equilibrium spin accumulation due to the momentum dependence of the Fermi ring spin texture $\mathbf{s}_{\mathbf{k}\nu}$. This result emerges naturally from the average of $\mathbf{s}_{\mathbf{k}\nu}$ away from equilibrium when considered in a semiclassical manner. To demonstrate this, let us consider the effect of small external perturbations upon the electron distribution function. The distribution function may then be written as $f_{\mathbf{k}\nu} + \delta f_{\mathbf{k}\nu}$, where $f_{\mathbf{k}\nu}$ is the Fermi function for the band ν,

$$\delta f_{\mathbf{k}\nu} \propto |\mathbf{E}| \sum_l \left[\tau_\parallel^{l,\nu} \cos(l\phi) + \tau_\perp^{l,\nu} \sin(l\phi) \right] \quad (29)$$

is the linear correction to $f_{\mathbf{p}\nu}$ due to the external electric field, and ϕ is the azimuthal angle of the momentum. Note that the coefficients $\tau_\parallel^{l,\nu}$ and $\tau_\perp^{l,\nu}$ are functions of α, m_z^2, and $|\mathbf{k}|$. The
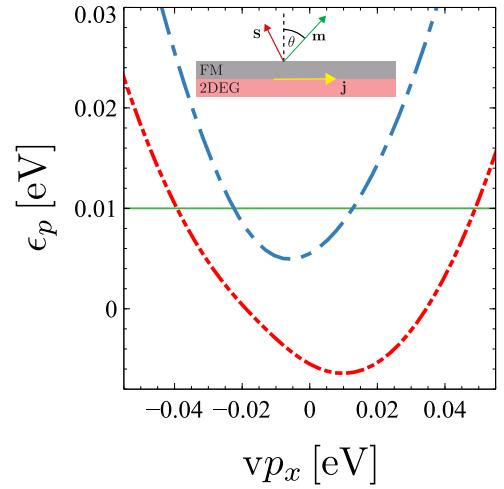

FIG. 2. Band structure of a two-dimensional electron gas (2DEG) with Rashba spin-orbit coupling (SOC) and an exchange interaction, where we have assumed $m_y = 0$ without loss of generality, which shifts the Fermi rings along the y axis by the m_x component. Parameters: $\alpha = 1.7 \times 10^{-11}$ eVm, $\Delta_{\text{xc}} = 5.5$ meV, $v = 10^5$ ms^{-1} (Fermi velocity), and $\theta = \pi/4$, and $p_y = 0$. The green line represents the Fermi energy $\varepsilon = 0.01$ eV. Inset: Normal metal (NM)/ferromagnet (FM) bilayer schematic, with electric current **J** aligned with the x axis and FM magnetization at angle θ to the z axis.

spin polarization is then given by

$$\mathbf{S} = \sum_{\mathbf{k},\nu} \mathbf{s}_{\mathbf{k}\nu} \, \delta f_{\mathbf{k}\nu}. \quad (30)$$

For a small in-plane magnetization, the spin texture of the 2DEG may be written as

$$\mathbf{s}_{\mathbf{k}\nu} = \nu \big(\mathbf{s}_{\mathbf{k}\nu}^0 + m_x \, \delta \mathbf{s}_{\mathbf{k}\nu} \big), \quad (31a)$$

$$\mathbf{s}_{\mathbf{k}\nu}^0 = \rho_\parallel \hat{\mathbf{k}} \times \mathbf{e}_z + \rho_\perp \mathbf{e}_z, \quad (31b)$$

$$\delta \mathbf{s}_{\mathbf{k}\nu} = [\omega_\parallel + \xi_\parallel \cos(2\phi)] \mathbf{e}_x$$
$$+ \xi_\parallel \sin(2\phi) \, \mathbf{e}_y - \omega_\perp m_z \sin\phi \, \mathbf{e}_z, \quad (31c)$$

where $\omega_{\parallel\perp}$, $\rho_{\parallel\perp}$, and $\xi_\parallel$ are functions of m_z^2, $|\mathbf{K}|$, and are linear in α. The $\mathbf{s}_{\mathbf{k}\nu}^0$ term is responsible for the spin-helical part of $\mathbf{s}_{\mathbf{k}\nu}$ and therefore produces an imbalance in oppositely aligned spins that is transverse to the applied electric field. Clearly, this term is the origin of the familiar REE, depending entirely on Rashba SOC, and generates nonzero contributions to K_{xy} and K_{yx}. These components survive the restrictions enforced by the FBA, where they appear independent of the magnetization.

We can easily see from Eq. (31) that the presence of an in-plane magnetization allows for an angle-dependent out-of-plane spin accumulation. Hence, this correction contributes to the K_{zx} and K_{zy} elements. However, under the FBA, we find that no such response is seen in the out-of-plane polarization S_z when $\varepsilon > \Delta_{\text{xc}}$ (i.e., when both of the spin-split bands are occupied), suggesting that the physics governing out-of-plane polarization is more sensitive to the scattering strength than REE. It turns out that the nonzero spin polarizations of the individual bands cancel out perfectly within the FBA, which
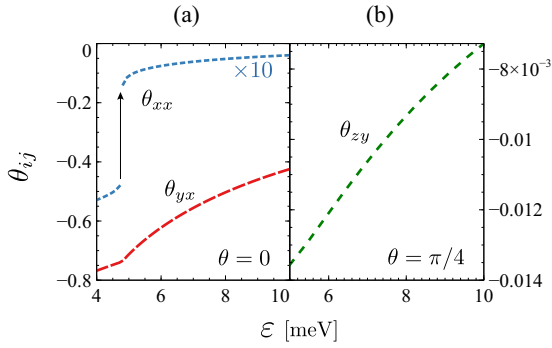
FIG. 3. Current-induced torque efficiencies as functions of the Fermi energy in the strong scattering limit, with magnetization (a) $\theta = 0$ and (b) $\theta = \pi/4$. In the former case, the range of Fermi energies covered spans both inside and outside the spin gap, whose upper limit is 4.8 meV, while in the latter, only the regime outside the spin gap is resolved. The blue lines portray the dampinglike torque efficiency, while the red and green curves represent the fieldlike torque efficiencies. Parameters: $m^* = 0.8m_e$, $\alpha = 1.7 \times 10^{-11}$ eVm, $\Delta_{xc}m_z = 4.8$ meV, and $n = 5 \times 10^{14}$ m^{-2}.

explains the vanishing of K_{zy} reported in Ref. [21]. Overall, there are four vanishing responses within the FBA, namely, $K_{zx} = K_{zy} = K_{xx} = K_{yy} = 0$.

To overcome the limitations of the FBA, we work with the scattering strength nonperturbatively by using the T-matrix approach detailed in Sec. II C; this allows for skew scattering when the partner FM has a finite out-of-plane magnetization component, i.e., $m_z \neq 0$. As a result, we find that the (k_x, k_y) and $(k_x, -k_y)$ points lying on the Fermi rings become inequivalent with different occupation numbers and hence generate a nonzero value for S_z. The same mechanism generates the diagonal contributions $K_{xx(yy)}$, which depend on m_z but to leading order are independent of m_x.

Next, we calculate the full spin-susceptibility tensor and the CSC efficiency. The disorder self-energy has the form:

$$\Sigma^{\pm} = \sum_{\alpha=0}^{3} n[g_\alpha(\varepsilon, \alpha, \mathbf{m}) \pm i\Gamma_\alpha(\varepsilon, \alpha, \mathbf{m})]s_\alpha, \quad (32)$$

where we note that the self-energy has now acquired a matrix structure (unlike in the Gaussian approximation), g_α and Γ_α are real functions, and $g_2 = \Gamma_2 = 0$. With this, we acquire the disorder-averaged Green's function by inserting Eq. (32) into Eq. (15), which in turn allows us to find $\hat{K}_J$ and hence the CSC efficiency. Further details of the calculations are provided in the Appendix. Going forward, we shall work in the limit of strong SOC, i.e., when the spin gap becomes well resolved within the quasiparticle broadening $n\Gamma_0 \ll \alpha p_F$, thus allowing for the efficient generation of nonequilibrium spin density. We may now start to analyze the DL and FL torques. We begin by considering how the CSC efficiency of the DL torque $\theta_{xx(yy)}$ depends on the Fermi energy for $m_x = 0$ within the strong scattering limit, which is shown in Fig. 3(a). Here, we see a discontinuity in $\theta_{xx(yy)}$, which can be attributed to breaching the upper limit of the spin gap, whereafter the magnitude of the CSC efficiency decreases monotonically and smoothly with increasing ε. This efficiency reduction can be explained by noting that the difference in occupation numbers of the two

Fermi rings becomes less significant by increasing the Fermi energy. In the large Fermi energy limit, there is a total overlap of the two Fermi rings that provide opposing contributions to $S_{x(y)}$; the result is a zero diagonal response.

For comparison, we present the FL CSC efficiency $\theta_{xy(yx)}$ also in Fig. 3(a). Here, we again see a monotonic decrease of the efficiency above of the spin gap, though the efficiencies are two orders of magnitude larger than their DL counterparts outside of the spin gap. Consequently, the SOT is dominated by the FL REE mechanism in this energy region. However, inside the spin gap, we find a giant DL response with $\theta_{xx(yy)}$ approaching 7% of the FL efficiency $\theta_{xy(yx)}$. Such a significant DL torque CSC efficiency cannot be achieved using perturbative methods, like the FBA and Gaussian approximations, which neglect skew scattering and therefore predict $K_{xx} = K_{yy} = K_{zx} = 0$ (and hence $\tau_{1,2}^e = 0$). Moving away from small in-plane magnetization, we find that K_{zy} renormalizes the FL SOT. We present the CSC efficiency of this term for $\theta = \pi/4$ in Fig. 3(b). We find that the K_{zy} term can reach up to 2% of the value of the REE FL terms in this case.

Let us now consider the WSL, where we may expand the response functions in powers of u. To write analytic expressions, we will need to assume a small in-plane magnetization, so we shall initially consider the regime $\Delta_x \ll \Delta_z \ll \alpha \ll \varepsilon$ and denote it by using a tilde. In this case, we expand the spin susceptibility to first order in m_x to yield

$$\widetilde{K} = -\frac{e}{2\pi n} \begin{bmatrix} -\frac{(m^*)^2 \Delta_z \alpha}{2\pi \varepsilon} & \frac{\alpha}{u^2} \\ -\frac{\alpha}{u^2} & -\frac{(m^*)^2 \Delta_z \alpha}{2\pi \varepsilon} \\ \frac{m^* \Delta_x \Delta_z^2}{4\pi \alpha \varepsilon^2} & -\frac{\Delta_x \Delta_z}{2\pi u \alpha \varepsilon} \end{bmatrix}, \quad (33)$$

where all elements are nonzero, as expected. We next note that $\sigma_{xx(yy)} = e^2\varepsilon/(\pi nm^* u^2)$ in the WSL for a large Fermi energy. Using Eqs. (4) and (33), we find the following torque efficiencies, $\tau_i^{e/o} = t_i^{e/o}/\sigma_{xx}$:

$$\tilde{\tau}_1^o = -\frac{m^*}{2e\varepsilon}\left(\alpha + \frac{\Delta_x^2 u}{2\pi \alpha \varepsilon}\right), \quad \tilde{\tau}_2^o = -\frac{m^* \Delta_{xc}^2 u}{4\pi e\alpha\varepsilon},$$

$$\tilde{\tau}_1^e = \frac{(m^*)^3 \Delta_{xc}\alpha u^2}{4\pi e\varepsilon^2}, \quad \tilde{\tau}_2^e = -\frac{(m^*)^2 \Delta_{xc} u^2}{4\pi e\varepsilon^2}\left(m^*\alpha - \frac{\Delta_z^2}{2\alpha\varepsilon}\right). \quad (34)$$

Equation (33) shows that the REE terms $(\tilde{K}_{xy}, \tilde{K}_{yx})$ are proportional to u^{-2} and are thus captured by the typical Gaussian white-noise distribution applied in the FBA. To capture the other entries, we consider the next order at u^{-1}, which requires the prescription of a non-Gaussian average of the form $\langle V(\mathbf{x})V(\mathbf{x}')V(\mathbf{x}'')\rangle = nR^6 u^3 \delta(\mathbf{x} - \mathbf{x}')\delta(\mathbf{x}' - \mathbf{x}'')$ [25]. The physics of this triple scattering within the response function is captured by truncating the T-matrix series at the third order in Fig. 1(b) [25]. Finally, the DL elements $\mathcal{O}(u^0)$ can be found by calculating fourth-order scattering diagrams.

An alternative regime to that above is one in which the SOC is weaker than the out-of-plane magnetization $\Delta_x \ll \alpha \ll \Delta_z \ll \varepsilon$, which we denote by an overline. In this case,
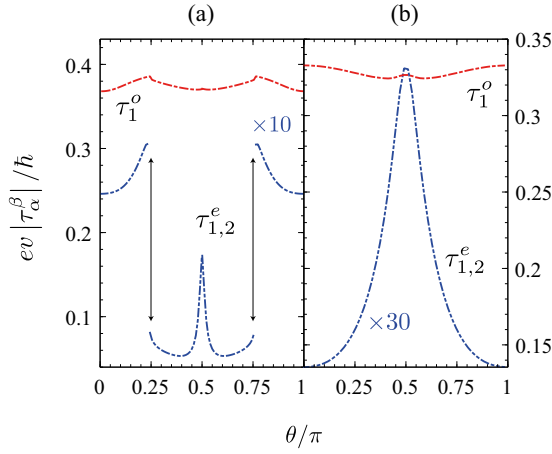
FIG. 4. Torque efficiencies as a function of magnetization angle, with periodicity π. The fieldlike torque efficiency τ_1^o is denoted by the red line, while the dampinglike efficiencies are equal in module, $|\tau_1^e| = |\tau_2^e|$, and represented by the blue line. In (a), the Fermi energy is inside the spin gap for $\theta = 0$, i.e., $\varepsilon = 4.5$ meV. The discontinuous behavior reflects the transition in the electronic band structure from inside to outside the spin gap. In (b), the Fermi energy is above the spin gap, $\varepsilon = 5.5$ meV, and the torque coefficients are smooth functions of θ. Parameters: $m^* = 0.8\, m_e$ (tantalum), $\alpha = 1.7 \times 10^{-11}$ eVm, $v = 5 \times 10^4\, \mathrm{ms}^{-1}$, $\Delta_{xc} = 5$ meV, and $n = 5 \times 10^{14}\, \mathrm{m}^{-2}$.

we find

$$\bar{K} = -\frac{e}{2\pi n}\begin{bmatrix} -\frac{(m^*)^3\alpha^3}{2\pi\Delta_z} & \frac{\alpha}{u^2} \\ -\frac{\alpha}{u^2} & -\frac{(m^*)^3\alpha^3}{2\pi\Delta_z} \\ \frac{(m^*)^2\alpha\Delta_x}{4\pi\epsilon} & -\frac{m^*\alpha\Delta_x}{2\pi u\Delta_z} \end{bmatrix}, \tag{35}$$

which yields

$$\bar{\tau}_1^o = -\frac{m^*\alpha}{2e\varepsilon}\left(1 + \frac{m^*\Delta_x^2 u}{2\pi\Delta_z^2}\right), \quad \bar{\tau}_2^o = -\frac{(m^*)^2\alpha\Delta_{xc}^2 u}{4\pi e\Delta_z^2\varepsilon},$$

$$\bar{\tau}_1^e = \frac{(m^*)^4\alpha^3\Delta_{xc} u^2}{4\pi e\Delta_z^2\varepsilon}, \quad \bar{\tau}_2^e = -\frac{\alpha(m^*)^3 u^2\Delta_{xc}}{4\pi e\varepsilon}\left(\frac{m^*\alpha^2}{\Delta_z^2} - \frac{1}{2\varepsilon}\right). \tag{36}$$

Next, we present the dominant FL and DL SOTs in Fig. 4 as functions of the magnetization angle θ in the strong scattering limit. We omit the τ_2^o contribution from these plots, as it is negligible compared with the τ_1^o contribution. The left panel [Fig. 4(a)] considers a Fermi energy inside the spin gap for an initial out-of-plane configuration of the magnetization. This is the *strong damping* regime, where the ratio between the DL and FL torques is maximized (see Fig. 3). As the magnetization of the FM is shifted from purely out-of-plane to purely in-plane (i.e., $\theta = 0 \rightarrow \pi/2$), the spin gap between the bands begins to shrink and vanishes when $\theta = \pi/2$. Consequently, the fixed Fermi energy will only intersect a single band for smaller angles, before then intersecting both bands at some *critical angle* $\theta_c(\varepsilon)$ ($\sim\pi/4$ in this case), where the spin gap has shrunk sufficiently to allow this, and hence, a discontinuity is observed at this $\theta_c(\varepsilon)$. This corresponds to moving from the strong damping regime to the *weak damping regime*. The angular dependence of the SOT coefficients is clearly symmetric about $\theta = \pi/2$. On the other hand, if the Fermi

energy is instead situated above the spin gap at $\theta = 0$, it will remain outside the spin gap for all magnetization angles, and hence, the system will always be in the weak damping regime. Therefore, the torque coefficients will be smooth continuous functions of θ, see Fig. 4(b). This complete angular description of $\tau_{1,2}^o$ and $\tau_{1,2}^e$ for strong disorder is enabled by treating the impurity potential and the magnetic exchange coupling on equal footing (i.e., a full T-matrix numerical treatment with a generic Δ_{xc}).

We can also see that, in both cases of Fig. 4, the standard FL contribution has a relatively weak angular dependence. Hence, τ_1^o may be treated as approximately constant to the first approximation, in line with previous literature [21]. In contrast, the DL torque coefficients, which are controlled entirely by the nonperturbative $K_{xx(yy)}$ components, exhibit a strong dependence upon the magnetization angle, a dependence that would otherwise be missed in perturbative methods. Clearly, the approximation of the DL torque coefficients as constants therefore breaks down.

IV. CONCLUSIONS

We have demonstrated that a complete understanding of DL torques in diffusive NM/FM bilayers hinges on scattering processes beyond the Gaussian approximation. Specifically, we showed that skew scattering is essential for a correct description of interfacial SOT already in diffusive systems characterized by impurities with weak scattering potentials. By treating both the disorder potential and spin-dependent interactions in the NM band structure nonperturbatively, we have gained access to SOTs in the strong scattering limit. Here, we found that ultrathin NM/FM bilayers host an efficient skew-scattering-activated DL SOT generated purely at the interface. This indicates that the bulk contribution to SOT (the SHE) is not a necessity for inducing magnetic switching of the FM, which may help shed light on recent experiments on ultrathin NM/FM bilayers, which observed SOT-driven switching of the magnetization of the FM [19].

As another application of the nonperturbative approach introduced here, we showed that the DL torque exhibited a nontrivial angular dependence upon the magnetization, thus illustrating the limitation of assuming the proximity-induced Zeeman coupling in the NM Hamiltonian to be completely out-of-plane (a common approximation in the literature). When the Fermi energy was located above the spin gap, we saw a dramatic increase in the DL torque as the out-of-plane magnetization approached zero. Similarly, for a Fermi energy inside the spin gap, we also observed a rapid increase in the DL torque, while the FL torque remained approximately constant. However, at some magnetization angle, a discontinuity in both the DL and FL torques was encountered due to the shrinking of the spin gap.

Given the scientific and technological importance of interfacial SOTs, the investigation of other exotic materials (e.g., topological insulators and Weyl semimetals) is of significant interest. What makes these materials so interesting is their unusual electronic structure and naturally strong SOC, which may give rise to a plethora of spin-charge interconversion processes. The formulation of a nonperturbative SOT theory

for those systems could unlock yet further manifestations of higher-order scattering processes.

APPENDIX

Here, we provide an outline of how to use functional programming within the Wolfram language to determine the electrical conductivity and spin susceptibility using the method introduced in Sec. II C:

(1) Determine the clean Green's function via simple matrix inversion $G_{0,\mathbf{p}}^{\pm} = (\varepsilon - H \pm \delta)^{-1}$, where δ is a positive infinitesimal and $H = \mathcal{H}_0 + \mathcal{H}_{PE}$.

(2) Obtain the momentum integrated Green's function, Eq. (16b): first perform direct angular integration of $G_{0,\mathbf{p}}^{\pm}$ and perform a partial fraction decomposition upon the result. This results in a sum of terms possessing the form $c(ak^2 + b)^{-n}$, where a, b, and c are all generic constants that depend upon ε, α, Δ_{xc}, and δ, while n is a positive integer. The remaining integral of these terms $\int dk\, k\, c(ak^2 + b)^{-n}$ is trivial, and so the radial momentum integral can be performed by using simple substitution rules with a UV cutoff $k_c = \Lambda/v$. Expand $g_0^{\pm}$ to leading order in order δ to obtain the appropriate form in the limit $\delta \to 0^+$.

(3) Construct the T-matrix and disorder-averaged Green's function using Eqs. (16a) and (15), respectively.

(4) Calculate all matrix elements of the Υ-matrix using the T-matrix obtained above.

(5) Calculate all matrix elements of the $\mathcal{N}$-matrix given the disorder-averaged calculations obtained in step (3). The momentum 2D integral here is handled in entirely the same fashion as in step (2), i.e., exact angular integration and the use of substitution rules to perform the radial integral. These results are then expanded to zeroth order in n due to the impurity density being a perturbative parameter (we work in the dilute impurity density limit).

(6) Construct the generalized Diffuson $\mathcal{D}$ and its analogous partner $\widetilde{\mathcal{D}}$ from the Υ-matrix and expanded $\mathcal{N}$-matrix.

(7) Finally, perform the momentum integrals in Eqs. (22) and (27) in the same manner as before to obtain the electrical conductivity and spin susceptibility, respectively.

As a final note regarding the nonperturbative numerical calculations performed to acquire Fig. 4, we follow a procedure analogous to that described above using the full T-matrix renormalization of the vertices. However, the key difference here is that we do not perform any expansion in terms of the impurity density when calculating the matrices $\mathcal{D}$ and $\widetilde{\mathcal{D}}$, and all integrals are performed numerically using standard methods.

[1] A. Manchon, J. Železný, I. M. Miron, T. Jungwirth, J. Sinova, A. Thiaville, K. Garello, and P. Gambardella, Rev. Mod. Phys. **91**, 035004 (2019).

[2] D. C. Ralph and M. D. Stiles, J. Magn. Magn. Mater. **320**, 1190 (2008).

[3] N. Locatelli, V. Cros, and J. Grollier, Nat. Mater. **13**, 11 (2014).

[4] R. Ramaswamy, J. M. Lee, K. Cai, and H. Yang, Appl. Phys. Rev. **5**, 031107 (2018).

[5] A. Brataas, A. D. Kent, and H. Ohno, Nat. Mater. **11**, 372 (2012).

[6] K. Garello, C. O. Avci, I. M. Miron, M. Baumgartner, A. Ghosh, S. Auffret, O. Boulle, G. Gaudin, and P. Gambardella, Appl. Phys. Lett. **105**, 212402 (2014).

[7] M. Cubukcu, O. Boulle, M. Drouard, K. Garello, C. Onur Avci, I. Mihai Miron, J. Langer, B. Ocker, P. Gambardella, and G. Gaudin, Appl. Phys. Lett. **104**, 042406 (2014).

[8] K. Dolui, M. D. Petrović, K. Zollner, P. Plecháč, J. Fabian, and B. K. Nikolić, Nano Lett. **20**, 2288 (2020).

[9] H. Liu, D. Bedau, D. Backes, J. A. Katine, J. Langer, and A. D. Kent, Appl. Phys. Lett. **97**, 242510 (2010).

[10] V. M. Edelstein, Solid State Commun. **73**, 233 (1990).

[11] R. H. Silsbee, Phys. Rev. B **63**, 155305 (2001).

[12] J. C. Rojas Sánchez, L. Vila, G. Desfonds, S. Gambarelli, J. P. Attané, J. M. De Teresa, C. Magén, and A. Fert, Nat. Commun. **4**, 2944 (2013).

[13] J.-i. Inoue, G. E. W. Bauer, and L. W. Molenkamp, Phys. Rev. B **67**, 033104 (2003).

[14] K. D. Belashchenko, A. A. Kovalev, and M. van Schilfgaarde, Phys. Rev. B **101**, 020407(R) (2020).

[15] V. P. Amin and M. D. Stiles, Phys. Rev. B **94**, 104420 (2016).

[16] S. Zhang, Phys. Rev. Lett. **85**, 393 (2000).

[17] C. Stamm, C. Murer, M. Berritta, J. Feng, M. Gabureac, P. M. Oppeneer, and P. Gambardella, Phys. Rev. Lett. **119**, 087203 (2017).

[18] K. Garello, I. M. Miron, C. O. Avci, F. Freimuth, Y. Mokrousov, S. Blügel, S. Auffret, O. Boulle, G. Gaudin, and P. Gambardella, Nat. Nanotechnol. **8**, 587 (2013).

[19] J. Kim, J. Sinha, M. Hayashi, M. Yamanouchi, S. Fukami, T. Suzuki, S. Mitani, and H. Ohno, Nat. Mater. **12**, 240 (2013).

[20] A. Manchon and S. Zhang, Phys. Rev. B **78**, 212405 (2008).

[21] I. A. Ado, O. A. Tretiakov, and M. Titov, Phys. Rev. B **95**, 094401 (2017).

[22] C. Xiao and Q. Niu, Phys. Rev. B **96**, 035423 (2017).

[23] C. Xiao and Q. Niu, Phys. Rev. B **96**, 045428 (2017).

[24] F. Sousa, G. Tatara, and A. Ferreira, Phys. Rev. Res. **2**, 043401 (2020).

[25] M. Milletarì and A. Ferreira, Phys. Rev. B **94**, 134202 (2016).

[26] M. Milletarì, M. Offidani, A. Ferreira, and R. Raimondi, Phys. Rev. Lett. **119**, 246801 (2017).

[27] M. Offidani, M. Milletarì, R. Raimondi, and A. Ferreira, Phys. Rev. Lett. **119**, 196801 (2017).

[28] M. Offidani and A. Ferreira, Phys. Rev. B **98**, 245408 (2018).

[29] M. Offidani and A. Ferreira, Phys. Rev. Lett. **121**, 126802 (2018).

[30] I. Miron, K. Garello, G. Gaudin, P.-J. Zermatten, M. Costache, S. Auffret, S. Bandiera, B. Rodmacq, A. Schuhl, and P. Gambardella, Nature (London) **476**, 189 (2011).

[31] X. Wang and A. Manchon, Phys. Rev. Lett. **108**, 117201 (2012).

[32] P. M. Haney, H.-W. Lee, K.-J. Lee, A. Manchon, and M. D. Stiles, Phys. Rev. B **87**, 174411 (2013).

[33] T. D. Skinner, M. Wang, A. T. Hindmarch, A. W. Rushforth, A. C. Irvine, D. Heiss, H. Kurebayashi, and A. J. Ferguson, Appl. Phys. Lett. **104**, 062401 (2014).

[34] I. Tokatly and E. Sherman, Ann. Phys. **325**, 1104 (2010).

[35] P. W. Anderson, J. Phys. C: Solid State Phys. **3**, 2436 (1970).

[36] C. Huang, M. Milletarì, and M. A. Cazalilla, Phys. Rev. B **96**, 205305 (2017).

[37] A. Crépieux and P. Bruno, Phys. Rev. B **64**, 014416 (2001).

[38] E. I. Rashba, Phys. Rev. B **68**, 241315(R) (2003).

[39] J. Rammer, *Quantum Transport Theory* (CRC Press, Boca Raton, 2004).

[40] M. Offidani, R. Raimondi, and A. Ferreira, Condensed Matter **3**, 18 (2018).

[41] P. J. Hirschfeld, P. Wölfle, and D. Einzel, Phys. Rev. B **37**, 83 (1988).

[42] A. Ferreira, T. G. Rappoport, M. A. Cazalilla, and A. H. Castro Neto, Phys. Rev. Lett. **112**, 066601 (2014).

[43] A. Ferreira, J. Phys. Mater. **4**, 045006 (2021).

[44] A. A. Burkov, A. S. Núñez, and A. H. MacDonald, Phys. Rev. B **70**, 155308 (2004).

[45] A. R. Mellnik, J. S. Lee, A. Richardella, J. L. Grab, P. J. Mintun, M. H. Fischer, A. Vaezi, A. Manchon, E.-A. Kim, N. Samarth *et al.*, Nature (London) **511**, 449 (2014).